The Astrophysical Journal, 952:159 (8pp), 2023 August 1 https://doi.org/10.3847/1538-4357/ace108

Electron Signal Induced by GRB 221009A on Charged Particle Telescopes of POES and MetOp Satellites

V. Vitale[1], C. Neubüser[2], R. Battiston[3], F. M. Follega[2,3], W. J. Burger[2], M. Babu[3], L. Conti[1,4], M. Cristoforetti[5], G. D'Angelo[6], C. Fidani[7], S. D'Arcangelo[7], M. Martucci[1], M. Mergè[8], A. Oliva[9], M. Orlando[7], A. Parmentier[6], M. Piersanti[10], D. Recchiuti[6], Z. Sahnoun[11,12], R. Sparvoli[1,13], and R. Iuppa[3]
[1] INFN—Sezione di Roma Tor Vergata, Via della Ricerca Scientifica 1, I-00133, Rome, Italy; vincenzo.vitale@roma2.infn.it
[2] TIFPA-INFN, Via Sommarive 14, I-38123 Trento, Italy
[3] University of Trento, Via Sommarive 14, I-38123 Trento, Italy
[4] Uninettuno University, C.so Via Emanuele II, 39, I-00186, Rome, Italy
[5] Fondazione Bruno Kessler, Via Sommarive 18, I-38123, Povo, Italy
[6] INAF-IAPS, Via Fosso del Cavaliere 100, I-00133, Rome, Italy
[7] INGV—Sezione di Roma 2, Via di Vigna Murata, 605, I-00143, Rome, Italy
[8] Italian Space Agency, Via del Politecnico, I-00133 Rome, Italy
[9] INFN—Sezione di Bologna, V.le Berti Pichat 6/2, Bologna, Italy
[10] University of L'Aquila, Via Vetoio, I-67100, L'Aquila, Italy
[11] Università di Bologna, V.le Berti Pichat 6/2, Bologna, Italy
[12] INFN—Sezione di Bologna, V.le Berti Pichat 6/2, Bologna, Italy
[13] University of Rome, Tor Vergata, I-38123 Rome, Italy
Received 2023 March 31; revised 2023 May 29; accepted 2023 June 21; published 2023 July 27

Abstract

GRB 221009A is a long gamma-ray burst among the most energetic and nearest ($z = 0.151$) detected so far. The energy fluence of the burst was so large to cause ionization of the upper layers of Earth's atmosphere and also observable signals in satellite-borne particle detectors. Electron signals, with the same GRB time development, can arise from the interaction of energetic photons with the particle detector and support structures. This effect was previously reported for the HEPP-L on board the China Seismo-Electromagnetic Satellite. We searched for the same effect on the particle detectors on board five POES and MetOp satellites. Electron signals in coincidence with the gamma-ray emission of the burst were found in three satellites, which were well illuminated by the GRB. The properties of the found electron signals are reported and discussed.

Unified Astronomy Thesaurus concepts: Gamma-ray bursts (629)

1. Introduction

Gamma-ray bursts (GRBs) are intense flashes of high-energy photons. They typically show a prompt phase followed by a longer afterglow emission. The prompt gamma-ray emission can last from a few up to hundreds of seconds and is thought to be produced by relativistic collimated plasma outflow launched by the rotating central engine (Kumar & Zhang 2015). The GRB afterglow is observable over a wide range of energies (from radio waves to very high-energy gamma rays). The low-energy component is thought to be produced by synchrotron radiation of relativistic electrons accelerated at the external shock wave (Rees & Mészáros 1992; Chiang & Dermer 1999), when the plasma propagates in the interstellar matter. In a fraction of GRBs, high-energy and very high-energy photons are observed both in the prompt and afterglow phases (Nava 2018). GRB 221009A was a long burst that has been observed by several orbiting X-ray and gamma-ray monitors and telescopes (Fermi GBM (Veres et al. 2022) and LAT (Bissaldi et al. 2022), Konus-Wind (Svinkin et al. 2022), AGILE (Ursi et al. 2022), INTEGRAL (Gotz et al. 2022), Insight-HXMT (Tan et al. 2022), GECAM-C (Liu et al. 2022), Neil Gehrels Swift Observatory (Swift), Monitor of All-sky X-ray Image (MAXI), and Neutron Star Interior Composition Explorer Mission (NICER) (Williams et al. 2023) and the CubeSat GRBAlpha (Ripa et al. 2023), and others). It was also detected by the LHAASO (Huang et al. 2022) ground array experiment, which reported the detection of thousands of very high-energy gamma rays, and at least one with energy of 18 TeV.

This burst was an utterly rare and energetic event. In Williams et al. 2023 it has been estimated that GRBs with similar energy and distance would occur at a rate of 1 per 1000 yr. This GRB was so intense to produce strong ionization on Earth's top atmospheric layers (Hayes & Gallagher 2022) and to induce observable effects even on space-borne particle detectors. Two possible mechanisms to create electron signals in the charged particle detectors are (i) electrons produced in the ionosphere, which do not have a very sharp time structure, since they drift for several tens to hundreds of seconds before reaching the telescopes and (ii) electrons from the direct interaction of energetic photons with the metal structures surrounding the particle detector silicon sensors, which are expected to exhibit the same GRB time structure. The first evidence of the latter mechanism has been reported in Battiston et al. 2023 where a strong electron signal has been observed by the HEPP-L charged particle detector on board the China Seismo-Electromagnetic Satellite (CSES-01). This prompt signal, closely modulated as the GRB photon flux time structure, can be explained through the direct interaction of the energetic photons with the particle detector structures. In this work, we searched for the same effect on the particle detectors on board the POES and MetOp satellites.

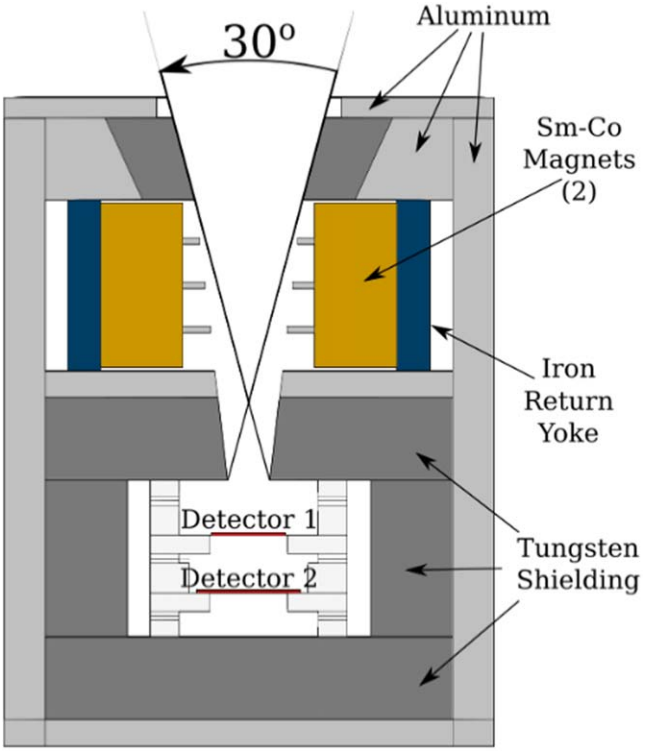

Figure 1. A schematic view of the MEPED proton telescope from Yando et al. (2011). The proton telescope includes a two silicon detector stack (each 200 μm thick) and a collimator with an angular half width of 15° and a similar inner collimator has a half width of 6.°5. Magnets (0.25 Tesla) deflect electrons. Electron telescopes are similar but they have a single silicon element 700 μm thick, which can fully contain incident electrons of energies up to ≈2500 keV, and no magnets, instead a nickel foil is used to block incident protons.

2. MEPED Instruments On Board the POES and MeTop Satellites

The Polar Orbiting Environmental Satellites (POES) is a constellation of satellites operated by the U.S. National Oceanic and Atmospheric Administration (NOAA). POES satellites are Sun synchronous with an orbit altitude of approximately 850 km, and a period of around 102 minutes. The European Organization for the Exploitation of Meteorological Satellites (EUMETSAT) also operates similar polar-orbiting satellites called the Meteorological Operational satellite (MetOp). In recent years, an average set of four or five satellites, belonging to the POES or MetOp fleets, were simultaneously operating. Each satellite of the POES, starting from POES 15, and of the MetOp series, carries a package particle detector called SEM-2 to measure the flux of energetic ions and electrons in orbit. The SEM-2 package includes the Total Energy Detector (TED) for the study of auroral particles, the Medium Energy Proton and Electron Detector (MEPED), to measure proton fluxes from 30 keV to 200 MeV, and electron ones from 30–2500 keV. Each MEPED consists of a pair of electron-directional telescopes, and a pair of proton ones. MEPED also has four omnidirectional detectors. The direction telescopes are oriented toward zenith (0°) and perpendicular to zenith (90°). The MEPED itself has an additional inclination angle of 9°. At the entrance of the electron telescope, there is a primary collimator with an angular half width of 15°, and a similar inner collimator with a half width of 6.°5 A nickel foil cover absorbs incident low-energy protons: 200–2700 keV protons are not rejected and constitute up to 20% of counts attributed to electrons. The passing particles are detected by a single 700 μm thick silicon detector, which can fully contain incident electrons with energies below 2500 keV (Yando et al. 2011). A schematic view of the MEPED proton telescope is reported in Figure 1.

Table 1
Energy Threshold (e.thr) and Geometric Factors (G) for Each of the MEPED Electron Telescopes

Electron Ch,	Energy Thr. (keV)	G (cm^2 s str keV)$^{-1}$	δG (cm^2 s str keV)$^{-1}$
E1	40	100/1.24	100/.64
E2	130	100/1.44	100/.32
E3	287	100/.75	100/.19
E4	612	100/.55	100/.40

Note. Data in the table are reproduced from the MEPED Telescope Data Processing Algorithm Theoretical Basis Document version 1.0, available at NCEI (www.ngdc.noaa.gov/stp/satellite/poes/dataaccess.html). Nominal energy thresholds are 30, 100, 300, and 600 keV. The reported effective thresholds are obtained with a dedicated analysis in the cited document. Note that the fourth electron channel (E4) is obtained with the sixth energy channel (P6) of proton telescopes, which are exploited also for the electron flux measurements.

2.1. GRB-induced Electron Signal

Large gamma-ray fluxes, such as the one of GRB 221009A, can produce a signal in orbital electron telescopes. via Compton scattering on the detector structural elements, followed by detection in the silicon detector. In Battiston et al. (2023), a simplified geometry of the space electron telescope HEPP-L, on board the CSES-01 satellite, was used, showing that secondary electrons can be detected (for the specific case of HEPP-L the secondaries originate in 83% of the cases in the passive material around the silicon, while about 17% are directly generated in the silicon detector). The geometry used in that work includes the silicon detectors and the nearby masses which are an aluminum collimator and an anticoincidence detector. Further modeling of the satellite and its masses was neglected as the large majority of the low-energy electrons produced in such masses do not reach the active detectors. Simulation results are general enough to be extrapolated for the MEPED telescopes. Both HEPP-L and the MEPED telescopes can be approximated by the geometry used and the differences in materials and structures dimensions do not significantly impact the secondary production mechanism.

Electron flux measurements above 600 keV (electron channel E4, see also Table 1) are obtained with proton telescopes. In comparing electron and proton telescopes results we consider that (i) for both types, the secondary electrons production follows the same mechanism, i.e., the majority of them are produced in the passive material around the silicon detector, and a smaller fraction in the detector itself; (ii) in the electron telescopes the induced secondaries are collected by a single 700 μm silicon chip, instead in the proton ones by two 200 μm chips; (iii) proton telescopes also have a magnet, and then more passive material; and (iv) the energy range above 600 keV, for which the proton telescopes are used, is less populated by secondaries. Given the several counteracting effects, a comprehensive comparison of electron and proton responses to induced secondary electrons would require detailed simulations of the two types of telescopes.

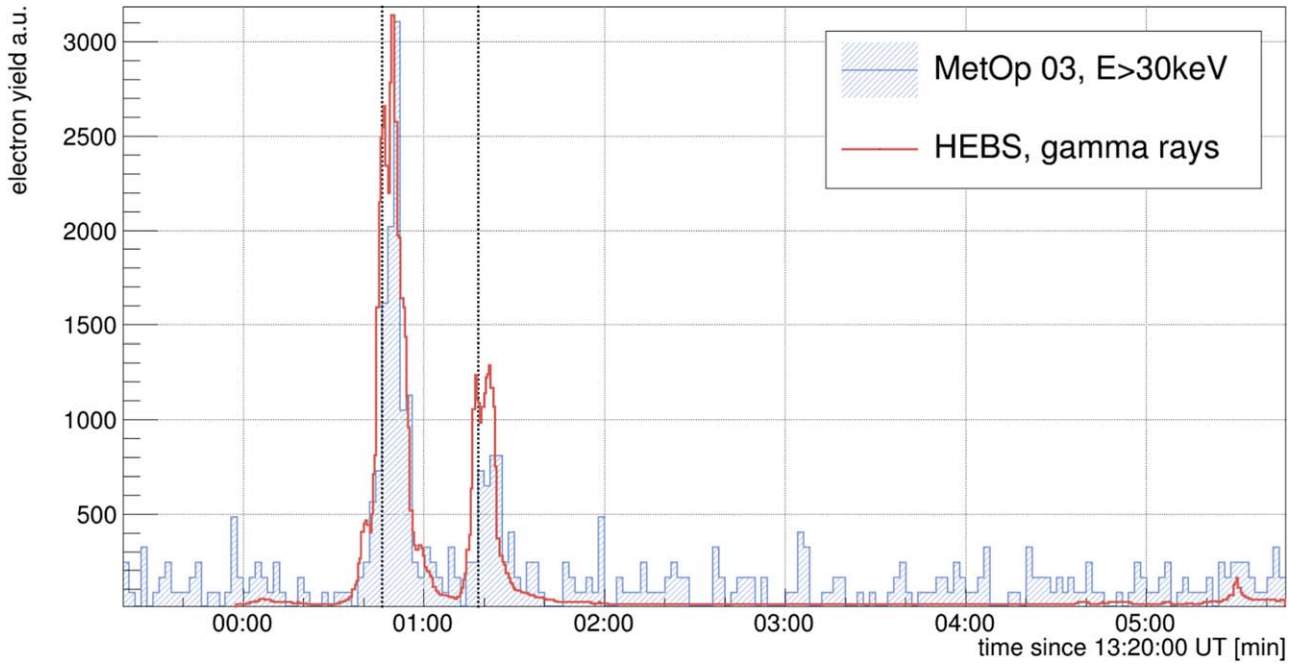

Figure 2. Electron yield detected with the 90° telescope of MetOp 03, for energy above 30 keV, in a time range of 5 minutes, after 13:20:00 UTC on 2022 October 9. The MetOp 03 data (black line, shadowed) are compared with the measured photon counts per second of the HEBS instrument (dark red line). HEBS data was scaled to match the MetOp 03 main peak. The two vertical dotted lines mark the rising edges of the first peak at 0:46.1 and of the second peak at 1:18.1

During normal operation, MEPED telescopes gather orbital electrons that have trajectories within their viewing cone. With the intense GRB 221009A, the MEPED electron telescopes are expected to record a mixture of orbital electron flux and GRB-induced electrons. The orbital electron flux acts as the background for the GRB signal. Therefore, the sensitivity of the MEPED telescopes to a GRB signal is expected to be dependent on both the GRB intensity and the intensity of the orbital electrons fluxes, which can vary by several orders of magnitude, being larger during polar passes and at the South Atlantic Anomaly (SAA).

3. Methods

The data collected with the MEPED telescopes on board the POES and MetOp satellites are distributed through the National Centers for Environmental Information (NCEI)[14], in the form of daily files. The distributed data include the electron fluxes, which are measured with each of the two telescopes (0° and 90°), in four integral energy channels (see Table 1). Among other information, the measurement time, the satellite position in longitude and latitude, its altitude, and the magnetic field intensity at the measurement position of the L-shells and the pitch angles, are provided. These data have a time cadence of 2 s.

In order to search for the signal induced by GRB 221009A we studied, by visual inspection, the electron fluxes. In this analysis, we searched for a significant excess in the same time range, in which orbital gamma-ray detectors measured the GRB emission. To associate the found excesses to the GRB emission, we also required a qualitative match between the light curve measured by the gamma-ray detectors and the time development of the electron fluxes, which are obtained with the MEPED telescopes (see Figure 2). We used the gamma-ray light curve produced by the High Energy Burst Searcher (HEBS; Liu et al. 2022; An et al. 2023), also known as GECAM-C, which is a gamma-ray monitor, working in the energy range 10 keV to 5 MeV, on board the SATech-01 microsatellite, launched in 2022 July. In the case of a sizable GRB effect, the electron telescopes record both GRB-induced electrons (ionization) and true orbital electrons; therefore, in the following plots we use the term *electron yield* for the electron telescope measurements.

4. Observations

The GRB 221009A was detected at 13:16:59.000 UT on 2022 October 9 (Veres et al. 2022). Figure 3 shows the positions of five satellites: POES 15, POES 18, POES 19, MetOp 01, and MetOp 03. These are the ones with an SEM-2 detector package active at the GRB time. Also reported on these maps are (i) the satellite's orbital trajectory during a time window of 40 minutes around the GRB; (ii) the first 6 minutes from 13:20:00 UTC, in color code; (iii) the region illuminated by the GRB, as a reddish area; (iv) in blue the area within the satellite's horizon. The GRB-illuminated region is calculated by considering a maximum angular distance of 90° from the point at 19°.8 and 71° in latitude and longitude, from which the GRB was seen at zenith. The satellite's horizon is obtained by tracing the tangent to the planet's surface, which intersects the satellite. The MEPED electron telescopes on the five mentioned satellites provide the following observations: (i) POES 19 shows only a marginal superposition between the area within the satellite's horizon and the GRB-illuminated one. Despite this, there is clear evidence of the main peaks in both the 0° and 90° telescopes, see Figure 4, similar to what has been found in Battiston et al. (2023). For POES 19, the 90° telescope has a relatively high background in the first tens of seconds; (ii) POES 15 was inside the GRB-illuminated area. Similarly to the previous satellite, it also had clear evidence of both of the main

[14] www.ngdc.noaa.gov/stp/satellite/poes/dataaccess.html

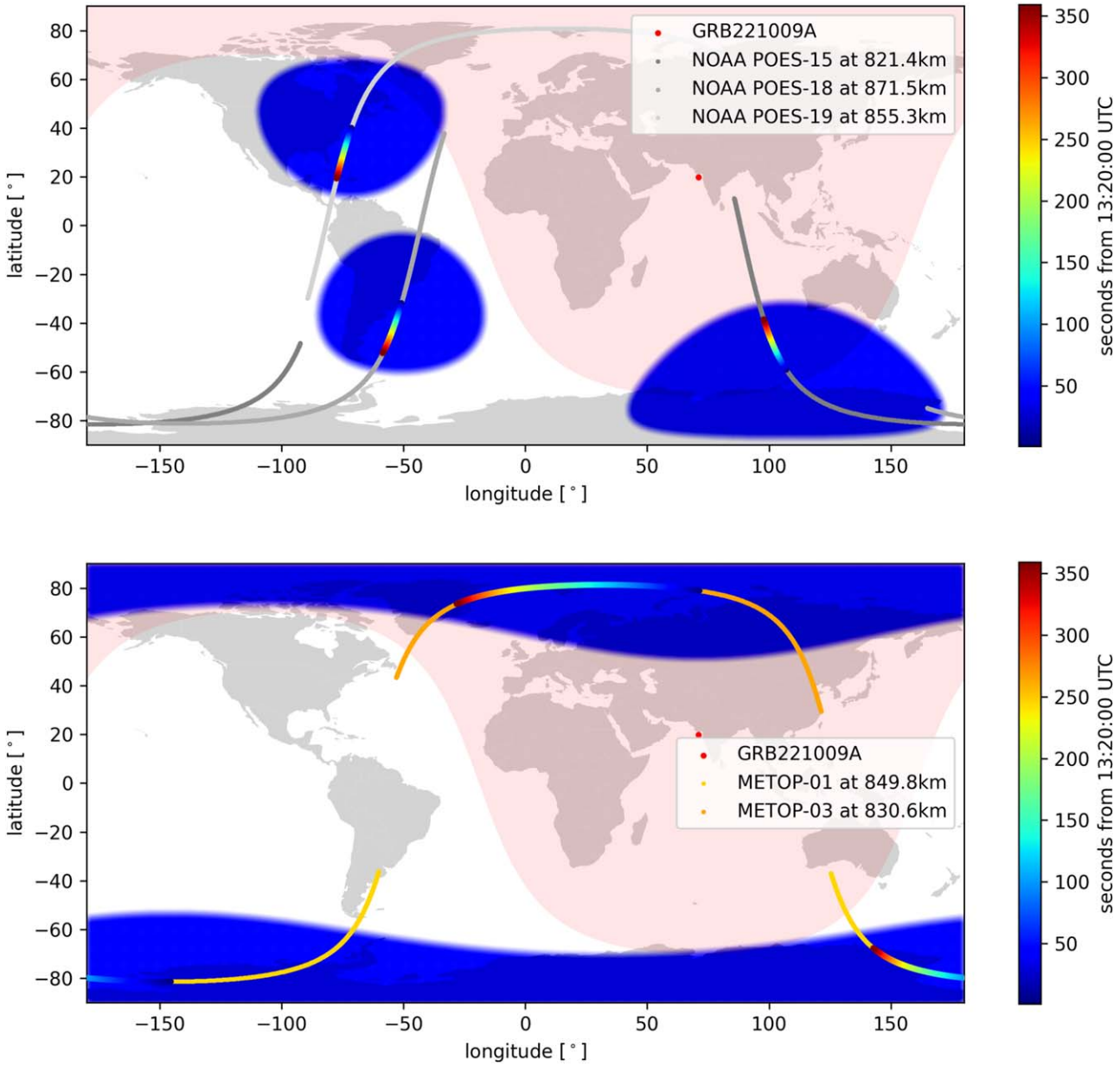

Figure 3. A map of Earth with the orbits of (a) NOAA POES satellites and the (b) NOAA MetOP 01 and 03 satellites shown in gray, on 2022 October 9 from 13:00–13:40 UTC. The color code along the orbit marks the seconds from 13:20:00 UTC for 6 minutes. The blue area corresponds to the satellite's view at the altitude, which is reported in the legend. The red-shaded area shows the approximate illumination area of GRB221009A, estimated for the central impact point (red dot) at 19.°8 and 71° in latitude and longitude, respectively.

peaks in both the 0° and 90° telescopes. The electron yield time profile is shown in Figure 5. In this case, 2 minutes after the t_0, the satellites entered a region of high background. Some peaks have multiple maxima but the second peak is likely polluted by background; (iii) MetOp 03 was inside the GRB-illuminated area. Its electron data exhibit a clear signal in both the 0° and 90° telescopes, for both the GRB main peaks as shown in Figure 6. The two time structures both exhibit a single maximum; (iv) MetOp 01 was outside the GRB-illuminated area. Despite several peaks in E1, within a time range from 40–100 s, it was not possible to identify a signal such as the one expected from GRB 221009A; and (v) POES 18 was outside the GRB-illuminated area and in a region of very high orbital flux because of the passage in the SAA.

Table 2 reports the timing for the main features of the electron yield time profile, associated with the GRB time structure. In MEPED data, every set of electron flux measurements is associated with a time stamp. These time stamps are all spaced by 2 s. They do not start exactly at the 00h:00s of the day, so that time stamps with decimal digits, such as those in Table 2, are provided. Furthermore, for each satellite, there is a specific offset from the 00h:00s of the day. The timing is performed only using the E1 channel for all the telescopes, as it provides larger statistics. Here the time reference t_0 is assumed to be 13:20:00 UTC on 2022 October 9. The reported features are (i) the rising edge of the first peak, e.g., the time when the electron yield reached half of its maximum; (ii) the time position of the First peak, which is the main structure in the time profile, starting approximately after

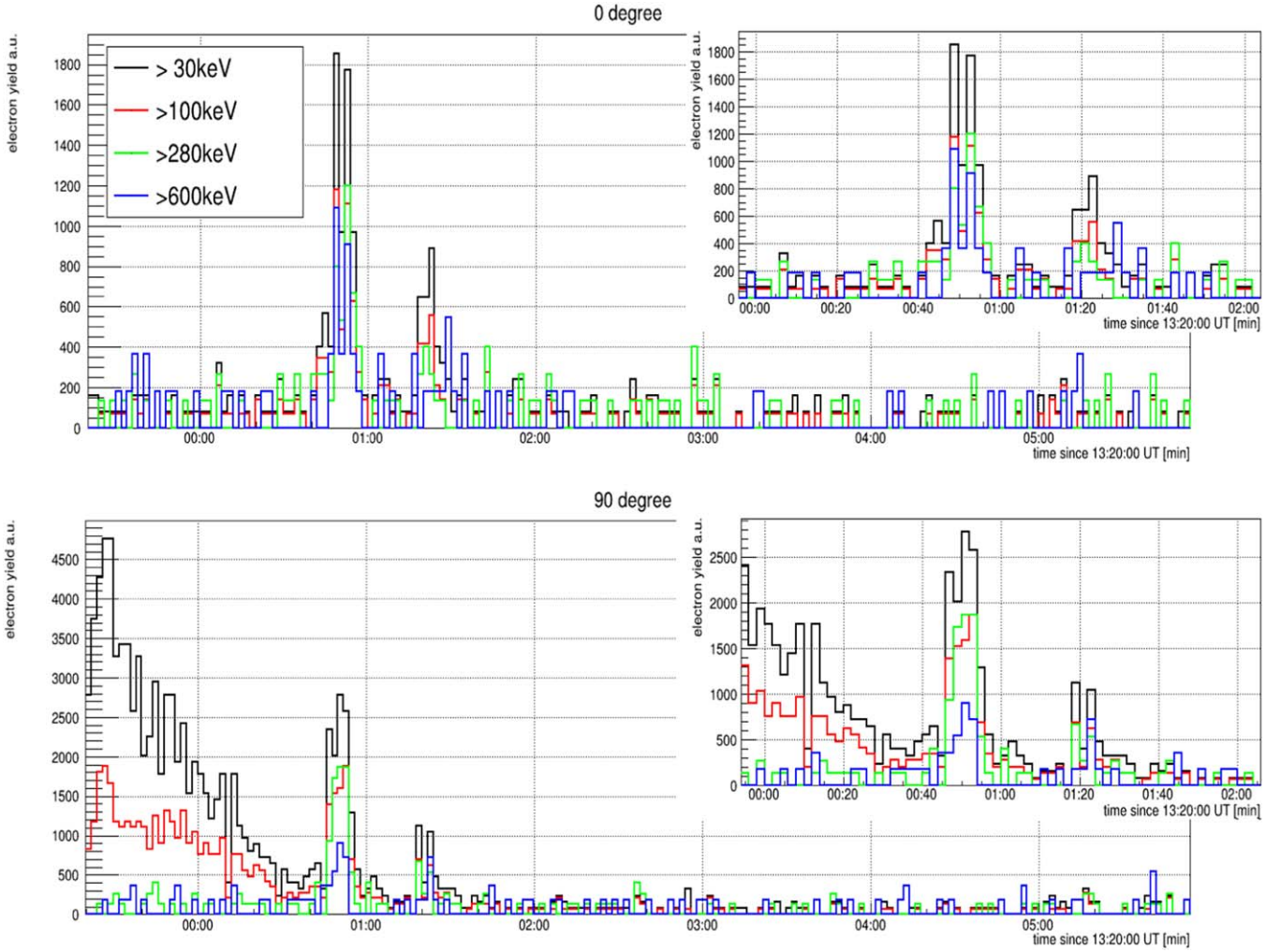

Figure 4. The detected electron yield vs. time for the MEPED telescopes on board the POES 19 satellite. Measurements in the time range of 5 minutes, after 13:20:00 UTC are reported. On the top, measurements made with the 0° telescope, on the bottom those of the 90° one. The color code indicates the four integral energy channels. In the inserts, a zoom of the first 2 minutes is reported.

Table 2
Features of the GRB221009A Light Curve, as Identified with the MEPED Data, Collected with the POES 19 (P19), POES 15 (P15), MetOp 03 (M03) Satellites

Telescope	Edge 1	Peak 1	Edge 2	Peak 2
M03-T0	0:46.1	0:49.1	1:20.1	1:23.1
M03-T90	0:46.1	0:51.1	1:18.1	1:24.8
P15-T0	0:47.9	0:48.9, 0:52.9	1:17.9	1:20.9, 1:24.9
P15-T90	0:45.9	0:48.9	1:15.9	1:18.9
P19-T0	0:47.9	0:48.9, 0:52.9	1:17.9	1:22.9
P19-T90	0:45.9	0:46.9, 0:50.9	1:17.9	1:18.9, 1:22.9

Note. Timing starts from 13:20:00 UTC on 2022 October 9. Measurements of the 0° telescope (T0) and of the 90° one (T90) are reported. The first and second peaks are visible in the data. For some telescopes, these peaks have two local maxima, which are both reported.

+46 s from t_0; (iii) the rising edge of the second peak, defined in the same way as for the first one; and (iv) the time position of the second peak, which is the smaller structure in the time profile, following the main peak and starting approximately at +77 to +80 s from t_0. The rising edges are less sensitive to statistics and background levels than the peak positions. In some cases, the peaks have two local maxima. All the first rising edges have times within 2 s, while the second rising edges are comprised of a slightly larger time interval.

In Table 3, we report the significance of each of the found peaks. The signal was searched in the time windows +43 to +49 s for the first peak and +75 to +87 s for the second one, considering small differences in the time stamp offset of the three satellites. The background was extracted in a time range where the orbital electron flux is dominant and steady. This time range was chosen as close as possible to the signal time windows, and goes from +0 s to +37 s for all the telescopes, while for POES-19 90°, the background was extracted in the interval +106.8 to +126.8 s (see Figure 4).

5. Conclusions

We searched for a signal of GRB 221009A in the MEPED telescope's electron measurements. Because the considered five satellites occupied different geographical positions at the GRB time, we observed both the effects of the different illumination by the GRB and of the different background levels. The GRB-induced signal was found in the three satellites, which are also those well illuminated by the GRB. The two main GRB peaks are evident in both the 0° and 90° telescopes, in almost all the

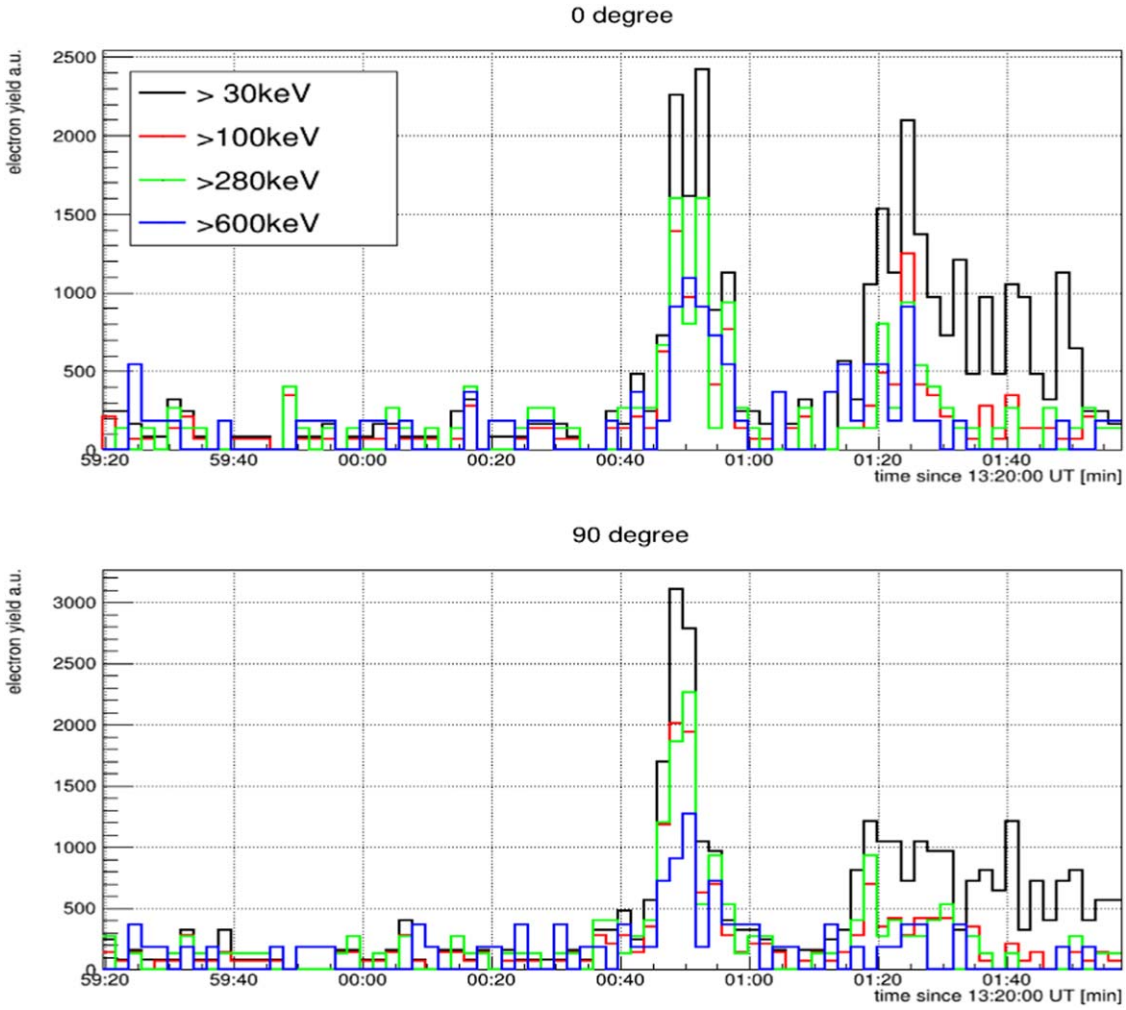

Figure 5. The detected electron yield vs. time for the MEPED telescopes on board the POES 15 satellite. Measurements in a time range of 2 minutes, after 13:20:00 UTC are reported; after that, the satellite entered a region with a much larger electron background. On the top, measurements made with the 0° telescope, on the bottom those of the 90° one. The color code indicates the four integral energy channels.

Table 3
The Significance of Each of the GRB Features Found

Telescope	Feature	E1	E2	E3	E4
		(σ)	(σ)	(σ)	(σ)
M03-T0					
	First peak	9.5	7.8	6.4	3.3
	Second peak	4.4	3.6		
M03-T90					
	First peak	10.0	8.4	7.8	5.1
	Second peak	5.1	3.8		
P15-T0					
	First peak	9.5	7.5	7.4	6.0
	Second peak *	8.7	4.9	4.4	4.7
P15-T90					
	First peak	10.4	8.4	8.8	6.0
	Second peak *	7.4	4.1	3.9	
P19-T0					
	First peak	8.2	6.5	6.1	5.2
	Second peak	4.7	4.2		
P19-T90					
	First peak *	11.4	9.1	8.9	4.6
	Second peak *	5.6	4.1	3.5	

energy channels, with E1 providing the best signal-to-noise ratio. The smaller third GRB peak, at 13:25:29 UTC, was not found.

We have found results very similar to the ones described in Battiston et al. (2023). That work reported a sub-second agreement between electron measurements and the GRB photon count time structure. That supported the interpretation of the interaction of gamma rays with the detector structure, as the source of the electron signal. With MEPED, the rising edge of the first peak was found between 46.1 and 47.9 s for the 0° telescopes, and between 45.9 and 46.1 s for the 90° telescopes. With the HEPP-L detector, in Battiston et al. (2023), the same time feature was reported at 45 s, then a few seconds earlier as compared to the average of MEPED results. In this respect, we note that (i) the MEPED data that we used have a 2 s cadence; and (ii) the time variable was associated by us to the center of the 2 s interval, during which the fluxes are measured. If instead, it marks the beginning or the end of such an interval, a systematic shift of ± 1 s is possible.

We also observed significances for each of the GRB features which are smaller than those obtained in Battiston et al. (2023). This might be due to the different thicknesses of the structures and size of the silicon detector between MEPED and HEPP-L,

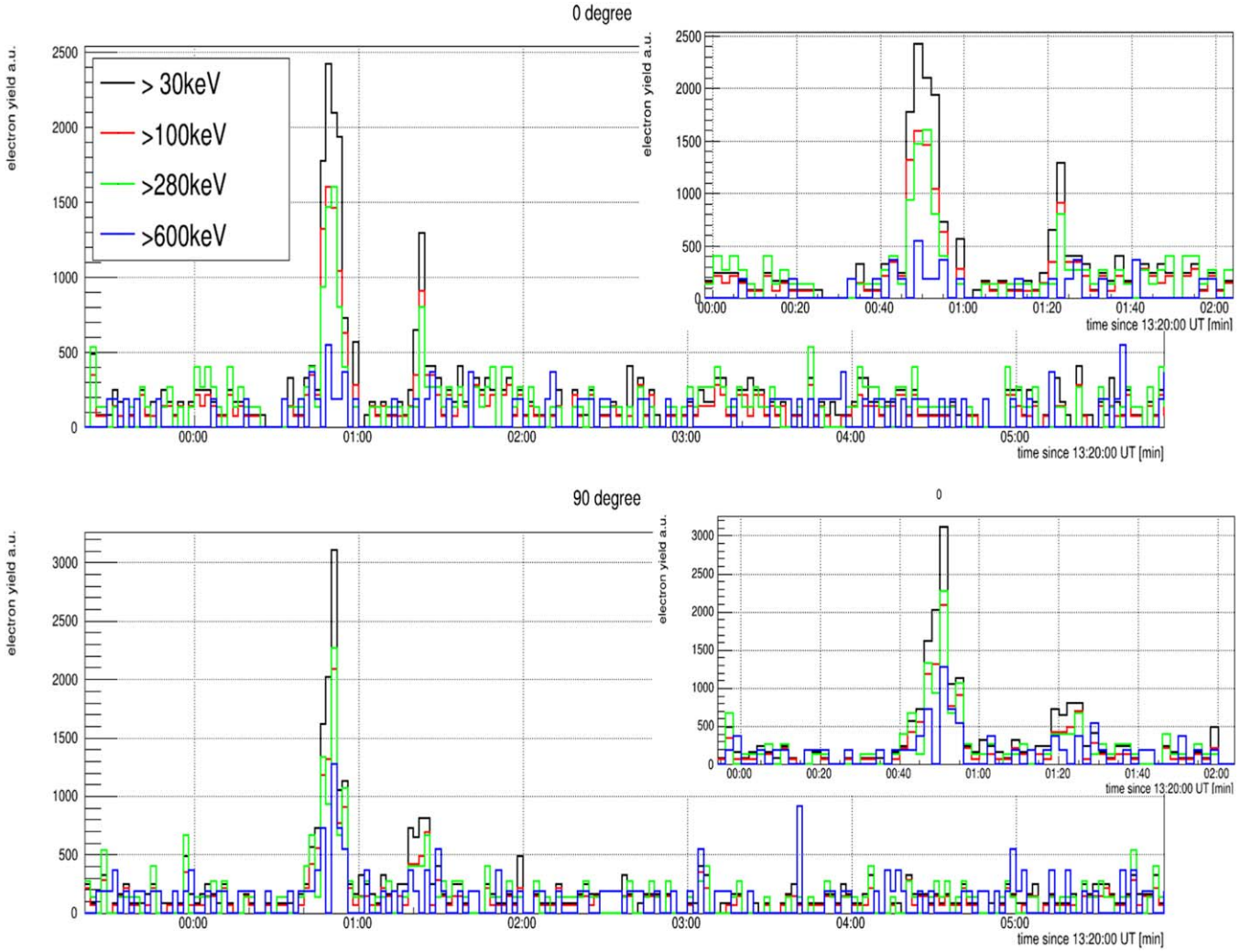

Figure 6. The detected electron yield vs. time for the MEPED telescopes on board the MetOp 03 satellite. Measurements in a time range of 5 minutes, after 13:20:00 UTC are reported. On the top, measurements made with the 0° telescope, on the bottom those of the 90° one. The color code indicates the four integral energy channels. In the inserts, a zoom of the first 2 minutes is reported.

which implies a different gamma-ray absorption and ionization efficiency. Another contribution to this difference could arise from the different amounts of gamma-ray flux shining directly over the silicon detectors, given the different orientations of the telescopes with respect to the GRB direction.

GRB 221009A is a very bright event with a fluence in the 15–150 keV band of $(7.4 \pm 0.1) \times 10^{-5}$ erg cm^{-2} (Williams et al. 2023). The very intense emission allowed us to detect the GRB main peaks, with adequate significance, and also with the MEPED electron telescopes, which are designed for other purposes. In general, the sensitivity of the MEDEP electron telescope to bright GRB is expected to be strongly dependent on the electron background, then on the orbital position. If we assume the same observational conditions as for GRB 221009A, then events with peak flux a factor of 4–5 lower can be detected with sufficient significance. Anyhow such events are bright and rare. It should be noted that (i) the sensitivity of the MEPED telescopes to a GRB signal can be largely reduced at large latitudes and during SAA passes; and (ii) the electron fluxes at Earth's orbit are significantly affected by several factors (such as geomagnetic storms, solar activity, etc.), which can produce structures in the time profile of electron measurements. Attempts to detect other gamma-ray signals with the MEPED detectors should take into consideration these features.

Acknowledgments

The authors thank the Italian Space Agency for the financial support under the contract ASI "LIMADOU Scienza+" No. 2020-31-HH.0. MEPED data obtained with the POES and MeTop satellites were provided by the NOAA through the NCEI.

ORCID iDs

V. Vitale https://orcid.org/0000-0001-8040-7852
C. Neubüser https://orcid.org/0000-0002-2008-8404
R. Battiston https://orcid.org/0000-0002-5808-7239
F. M. Follega https://orcid.org/0000-0003-2317-9560
R. Iuppa https://orcid.org/0000-0001-5038-2762

References

An, Z.-H., Antier, S., Bi, X.-Z., et al. 2023, arXiv:2303.01203
Battiston, R., Neubüser, C., Follega, F. M., et al. 2023, ApJL, 946, L29
Bissaldi, E., Omodei, N., Kerr, M. & (Fermi-LAT Team) 2022, GCN, 32637, 1
Chiang, J., & Dermer, C. D. 1999, ApJ, 512, 699
Gotz, D., Mereghetti, S., Savchenko, V., et al. 2022, GCN, 32660, 1

Hayes, L. A., & Gallagher, P. T. 2022, RNAAS, 6, 222
Huang, Y., Hu, S., Chen, S., et al. 2022, GCN, 32677, 1
Kumar, P., & Zang, B. 2015, PhR, 561, 1
Liu, J. C., Zhang, Y. Q., Xiong, S. L., et al. 2022, GCN, 32751
Nava, L. 2018, IJMPD, 27, 1842003
Rees, M. J., & Mészáros, P. 1992, MNRAS, 258, 41
Ripa, J., Takahashi, H., Fukazawa, Y., et al. 2023, arXiv:2302.10047
Svinkin, D., Frederiks, D., Ridnaia, A., et al. 2022, GCN, 32641, 1
Tan, W. J., Li, C. K., Ge, M. Y., et al. 2022, ATel, 15660, 1
Ursi, A., Panebianco, G., Pittori, C., et al. 2022, GCN, 32650, 1
Veres, P., Burns, E., Bissaldi, E., et al. 2022, GCN, 32636, 1
Williams, M. A., Kennea, J. A., Dichiara, S., et al. 2023, ApJL, 946, L24
Yando, K., Millan, R. M., Green, J. C., & Evans, D. S. 2011, JGRA, 116, A10231